

# Indefinite causal order in a quantum switch

K. Goswami,<sup>1</sup> C. Giarmatzi,<sup>1</sup> M. Kewming,<sup>1</sup>  
F. Costa,<sup>1</sup> C. Branciard,<sup>2,\*</sup> J. Romero,<sup>1,†</sup> and A. G. White<sup>1,‡</sup>

<sup>1</sup>Centre for Engineered Quantum Systems, School of Mathematics and Physics, University of Queensland, QLD 4072 Australia

<sup>2</sup>Univ. Grenoble Alpes, CNRS, Grenoble INP, Institut Néel, 38000 Grenoble, France

(Dated: December 3, 2024)

In quantum mechanics events can happen in no definite causal order: in practice this can be verified by measuring a causal witness, in the same way that an entanglement witness verifies entanglement. Indefinite causal order can be observed in a quantum switch, where two operations act in a quantum superposition of the two possible orders. Here we realise a photonic quantum switch, where polarisation coherently controls the order of two operations,  $\hat{A}$  and  $\hat{B}$ , on the transverse spatial mode of the photons. Our setup avoids the limitations of earlier implementations: the operations cannot be distinguished by spatial or temporal position. We show that our quantum switch has no definite causal order, by constructing a causal witness and measuring its value to be 18 standard deviations beyond the definite-order bound.

In daily experience, it is natural to think of events happening in a fixed causal order. Strikingly, it has been proposed that quantum physics allows for nonclassical causal structures where the order of events is *indefinite* [1, 2]. It has been theoretically shown that such a possibility provides an advantage for computation [3], communication complexity [4, 5] and other information processing tasks [6–8]. Furthermore, investigations of indefinite causal orders suggest a promising route towards a theory that combines general relativity and quantum mechanics [9, 10].

Indefinite causal orders can be studied using a framework that distinguishes whether some experimental situation—called a *process*—is compatible with a fixed causal order of the events or not. An example of a process with indefinite causal order is the *quantum switch* [1]. In the quantum switch, the order in which two “black box” operations are performed on a target system is coherently controlled by a control quantum system, Fig. 1(a–c). The advantages provided by the quantum switch arise from the fact that it cannot be reproduced by an ordinary quantum circuit which uses the same number of black-box operations [3–7].

In light of the possible practical applications, it is important to understand whether the quantum switch can be realised in the laboratory. Recent proof-of-principle implementations [11, 12] do not realise the switch advantage in practice as they use additional black-boxes. In those implementations, the order is controlled by the path taken by the photons, while each black box—a set of waveplates—acts on their polarisation. This means that the photons pass through the waveplates at two *different* spatial locations, depending on the order. These are distinct operations, as can be seen by slicing the waveplates, Fig. 1(d). Further, the photons used in these implementations have a coherence length much shorter than the distance between the two sets of waveplates: in effect, the operations could also be distinct in time, since one could perform different operations with fast control of

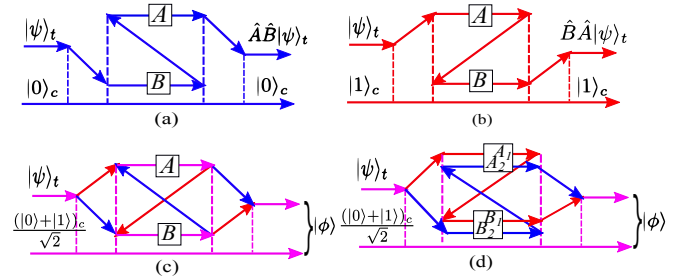


FIG. 1. The *quantum switch*. A control qubit determines the order in which two quantum operations,  $\hat{A}$  and  $\hat{B}$  are applied to a target qubit,  $|\psi\rangle_t$ . (a) When the control is in the state  $|0\rangle_c$ , the resulting operation is  $\hat{A}\hat{B}$ , while (b) when the control is in the state  $|1\rangle_c$ , the operation is  $\hat{B}\hat{A}$ . (c) With the control qubit in a quantum superposition  $\frac{1}{\sqrt{2}}(|0\rangle + |1\rangle)_c$ , the order of the operations is also in a superposition so that the joint state of the control and target systems at the output of the quantum switch is  $|\phi\rangle = \frac{1}{\sqrt{2}}(\hat{A}\hat{B}|\psi\rangle_t \otimes |0\rangle_c + \hat{B}\hat{A}|\psi\rangle_t \otimes |1\rangle_c)$ . (d) In Refs. [11, 12],  $|\psi\rangle_t$  is encoded in the polarisation degree of freedom, while  $|0\rangle_c$  and  $|1\rangle_c$  correspond to different paths through the waveplates that realise the operations  $\hat{A}$  and  $\hat{B}$ . As the photons are incident at two different points on each of the waveplates, the circuit realises four different operations,  $\hat{A}_1$ ,  $\hat{A}_2$ , and  $\hat{B}_1$ ,  $\hat{B}_2$ .

the waveplates.

Here we overcome these limitations to realise a quantum switch with only two black boxes; further, each black box is only used once. We introduce a causal witness [13, 14] and use it to verify indefinite causal order, 18 standard deviations beyond definite ordering. Our implementation, in which the control and target qubits are encoded in the polarisation and in the transverse spatial mode of a photon, respectively, opens the possibility of encoding more than two levels in the target system—which is useful, for example, in communication tasks with advantages over definite causal ordering [5, 8].

Much of the interest in the quantum switch comes from the possibility of representing a novel—genuinely quantum—type of causal structure. In this context, causal relations are defined through the possibility of

transmitting signals between events. An *event* is understood operationally in terms of operations such as measurements, preparations, or transformations of a physical system (for example, a photon transiting a set of lenses can define an event). A *causal structure* represents the network of possible causal relations between a set of events. Relativistic causal structure naturally falls within this perspective: if an event  $A$  is in the past light-cone of an event  $B$  it is possible to send a signal from  $A$  to  $B$ , while no signal exchange is allowed for space-like separated events. Note that, even if no direct causal influence between certain events is detected in a given experiment, it might still be possible to deduce information about the causal structure in which the events are embedded. For example, one can perform transformations on a system at the prescribed events and, by measuring the system at a later event, deduce information about the order in which the transformations were applied. Our experiment will use this idea.

Since the notion of causal structure refers to how different operations on physical systems relate to each other, distinct definitions are available depending on the level of description of these operations and of the physical systems. Recent literature [2, 13–16] has analysed the quantum causal structure of the quantum switch using a theory- and device-dependent approach: we follow this here. The possible operations defining an event  $A$  are identified with the most general quantum operations: completely positive (CP) maps from an input space,  $A_I \equiv \mathcal{L}(\mathcal{H}^{A_I})$  to an output space,  $A_O \equiv \mathcal{L}(\mathcal{H}^{A_O})$ , where  $\mathcal{L}(\mathcal{H})$  denotes the space of linear operators over a Hilbert space  $\mathcal{H}$  and  $A_I, A_O$  label the spaces attached to the system immediately before and after the operation, respectively. Using the Choi-Jamiołkowski isomorphism [17, 18] we represent a CP map as a positive semidefinite operator  $M^A \in A_I \otimes A_O$ . The probability to realise the maps  $\{M^A, M^B, \dots\}$  in an experiment, corresponding to the events  $A, B, \dots$ , is given by the *generalised Born rule* [2, 19–21]

$$P(M^A, M^B, \dots) = \text{Tr}[(M^A \otimes M^B \otimes \dots) W], \quad (1)$$

where  $W \in A_I \otimes A_O \otimes B_I \otimes B_O \otimes \dots$  is a positive semidefinite matrix called a *process matrix*, which provides a full specification of the possible correlations that can be observed. In particular,  $W$  encodes the causal structure, namely which events can potentially influence which other events.

Three events  $A, B$  and  $C$  must be identified in a quantum switch:  $A$  and  $B$  correspond to operations on the target system implemented along the two arms of the interferometer, while  $C$  is a measurement on the control system that occurs after both events  $A$  and  $B$  (not shown in Fig. 1; see Fig. 2). A process matrix compatible with  $A$  causally preceding  $B$  is denoted  $W^{A \prec B \prec C}$ ; a process matrix with  $B$  preceding  $A$  is denoted  $W^{B \prec A \prec C}$ . If a causal order between the events is well defined for each

run of the experiment, possibly changing randomly between different runs, then the process matrix is said to be *causally separable* [2, 13, 15] and it can be decomposed in the form

$$W_{\text{sep}} = q W^{A \prec B \prec C} + (1 - q) W^{B \prec A \prec C}, \quad (2)$$

where  $0 \leq q \leq 1$ .

Our task is to experimentally verify an indefinite causal order, namely that the process matrix describing our experiment cannot be decomposed as in Eq. (2). We achieve this by measuring a *causal witness* [13, 14]. This is defined as a Hermitian operator  $S$  such that its expectation value is

$$\langle S \rangle = \text{Tr}[S W_{\text{sep}}] \geq 0 \quad (3)$$

for every causally separable process matrix  $W_{\text{sep}}$ . Detecting a value  $\langle S \rangle = \text{Tr}[S W] < 0$  therefore certifies that  $W$  is *causally nonseparable*.

Notice that the value of  $\text{Tr}[S W]$  can be obtained experimentally after decomposing  $S$  into different operators representing different CP maps (which define the events  $A, B, C$ ), and using Eq. (1) to write  $\text{Tr}[S W]$  as a combination of the joint probabilities of these maps to be realised. In our experiment, we use a causal witness that can be measured by letting events  $A$  and  $B$  correspond to unitary operations  $\hat{A}$  and  $\hat{B}$ , respectively, and event  $C$  to a polarisation measurement of the control qubit in the diagonal/antidiagonal basis—i.e., a measurement of a Stokes parameter, or equivalently of the Pauli observable  $\hat{X}$ . Such a witness can be decomposed as

$$S = \frac{1}{4} \left( \hat{I} + \sum_{\hat{A}, \hat{B}} \gamma_{\hat{A}, \hat{B}} \mathcal{A} \otimes \mathcal{B} \otimes \hat{X} \right), \quad (4)$$

where  $\hat{I}$  denotes the identity operator,  $\mathcal{A}$  is the Choi representation of a unitary  $\hat{A}$ , defined as  $\mathcal{A} := (\sum_{lm} |l\rangle\langle m| \otimes \hat{A} |l\rangle\langle m| \hat{A}^\dagger)^T$  (where  $T$  denotes transposition in the computational basis  $\{|l\rangle\}$  of  $\mathcal{H}^{A_I}$ ), similarly for  $\mathcal{B}$ , and where the sum runs over the sets of unitaries  $\hat{A}, \hat{B}$  used in the experiment. The normalisation factor  $\frac{1}{4}$  is chosen so that the value of  $-\text{Tr}[S W]$ , when positive (i.e., when  $\text{Tr}[S W] < 0$ ), corresponds precisely to the amount of white noise that can be added to  $W$  before it becomes causally separable (its “random robustness”) [13, 14], and the coefficients  $\gamma_{\hat{A}, \hat{B}}$  are determined numerically through the optimisation method described in the Supplemental Material. The value we need to measure is then

$$\begin{aligned} \langle S \rangle &= \text{Tr} \left[ \frac{1}{4} \left( \hat{I} + \sum_{\hat{A}, \hat{B}} \gamma_{\hat{A}, \hat{B}} \mathcal{A} \otimes \mathcal{B} \otimes \hat{X} \right) W_{\text{exp}} \right] \\ &= 1 + \frac{1}{4} \sum_{\hat{A}, \hat{B}} \gamma_{\hat{A}, \hat{B}} \langle \hat{X} \rangle_{\hat{A}, \hat{B}}, \end{aligned} \quad (5)$$

where  $W_{\text{exp}}$  is the process matrix describing our experiment (properly normalised so that  $\text{Tr} W_{\text{exp}} = 4$  for our

quantum switch [13–15]) and  $\langle \hat{X} \rangle_{\hat{A}, \hat{B}}$  is the expectation value of the observable  $\hat{X}$  given that  $\hat{A}$  and  $\hat{B}$  have been performed. If  $\langle S \rangle$  is found to be negative, it means that our implementation of the quantum switch has successfully realised an indefinite causal order between the events  $A$  and  $B$ .

To overcome the spatial-separation loophole left open in Refs. [11, 12], we use polarisation as the control qubit for the order of black boxes and the transverse spatial mode of the photons as our target qubit. With this encoding there is a single optical axis throughout the quantum switch, meaning that each black box cannot be spatially split into two. We overcome the temporal loophole by using photons of long coherence length. The spatial separation between the input and output of black boxes  $A$  and  $B$  in Fig. 2 is 3.5 m and two orders of magnitude shorter than the coherence length of our light source which is 955 m, such that no significant timing information can be derived.

Our light source is a diagonally-polarised, 100 kHz linewidth laser beam at 795 nm, in the lowest-order transverse spatial mode (the Hermite-Gaussian mode  $\text{HG}_{00}$ ). We transform the beam into a  $\text{HG}_{10}$  spatial mode by first passing the beam through an element that adds a  $\pi$ -phase to half of the beam (a cover slip on a tip-tilt mount that spans half of the beam). The resulting spatial mode is a superposition of odd-order Hermite-Gaussian modes [22]. We then use spatial Fourier filtering to remove most of the higher-order spatial modes leaving just the  $\text{HG}_{10}$  mode. The qubit space of the target system consists of first-order spatial modes, where we define  $|0\rangle = |\text{HG}_{10}\rangle$ , and  $|1\rangle = |\text{HG}_{01}\rangle$ . The initial state of  $|\psi\rangle_t$  is taken to be  $|0\rangle$  (Fig. 1).

A polarising beamsplitter (PBS1) splits the beam into the top and bottom arms of an interferometer, see Fig. 2. The unitary operations in these arms,  $\hat{A}$  and  $\hat{B}$ , act on the transverse spatial mode, but should (ideally) not change the polarisation of the beam. The top and bottom arms are combined at the output polarising beamsplitter, PBS2, and the resulting mode is sent back to the other input of PBS1; this relay arm contains a telescope to ensure mode-matching, i.e., that the spatial mode that re-enters the interferometer is the same as the input spatial mode.

We realise the unitary operations  $\hat{A}$  and  $\hat{B}$  using a combination of inverting prisms [23] and cylindrical lenses [24, 25] as shown in Fig. 3. The inverting prisms rotate the incoming spatial mode. Unlike Dove prisms which act as poor polarisers [26], an inverting prism acts approximately as a quarter-waveplate [23], which we compensate using a combination of quarter- and half-waveplates.

Transformations for spatial modes require more optical elements than transformations for polarisation, hence in constructing the witness, we considered a tradeoff be-

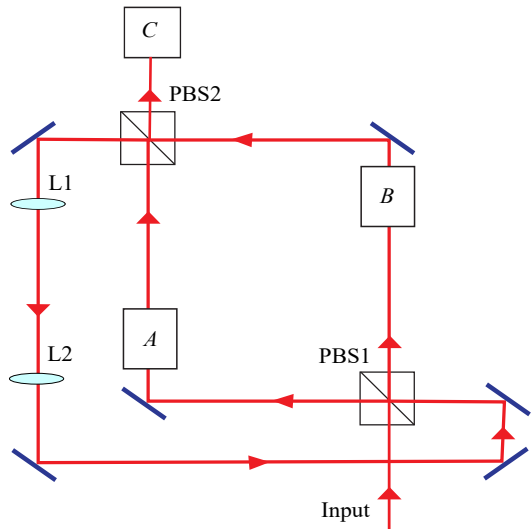


FIG. 2. Experimental schematic. The control qubit is defined by polarisation. The polarising beamsplitter PBS1 routes the photon into either events  $A$  or  $B$ , which realise unitary operations  $\hat{A}$  or  $\hat{B}$  acting on the spatial mode of the photon. Event  $C$  is a  $\hat{X}$  polarisation measurement, determining the Stokes parameter of the photon in the diagonal/anti-diagonal basis. Lenses  $L1$  and  $L2$  are used as a telescope to ensure mode-matching.

tween its robustness to noise and the number of elements required to measure it in our setup. For this reason, in our experiment each operation  $\hat{A}$  and  $\hat{B}$  is chosen among one of the following six unitaries acting on the transverse spatial mode: the identity operation  $\hat{I}$ , the three Pauli operators  $\hat{X}$ ,  $\hat{Y}$  and  $\hat{Z}$ , and the two linear combinations  $\hat{P} = (\hat{Y} + \hat{Z})/\sqrt{2}$  and  $\hat{Q} = (\hat{X} + \hat{Z})/\sqrt{2}$ . These operations produce spatial modes that are either first-order Hermite-Gaussian or first-order Laguerre-Gaussian modes (thus keeping the spatial mode in the  $\{|\text{HG}_{10}\rangle, |\text{HG}_{01}\rangle\}$  qubit subspace). Fig. 4 illustrates the resulting spatial modes for an input target qubit in the  $\text{HG}_{10}$  mode.

At the interferometer output, after PBS2, event  $C$  corresponds to a polarisation measurement in the diagonal/antidiagonal basis (a measurement of the Stokes parameter corresponding to  $\langle \hat{X} \rangle$ ), selected using a half-waveplate and a third polarising beamsplitter. Due to experimental imperfections in the optical elements, the output mode has a marked transverse interference pattern, typically with two to three fringes. An iris is used to collect only light from one fringe, and this is then collected by a multimode fibre connected to a single-photon detector, thus tracing out the spatial mode of the photons.

For our witness, there are 21 combinations of  $\hat{A}$  and  $\hat{B}$  for which the coefficient  $\gamma_{\hat{A}, \hat{B}}$  is nonzero (see Supplemental Material). Fig. 5 shows the measured Stokes values  $\langle \hat{X} \rangle_{\hat{A}, \hat{B}}$  for each of these combinations: the red bars are the theoretically expected values, which should all be +1, -1 or 0; the blue bars are the values measured in our experiment.

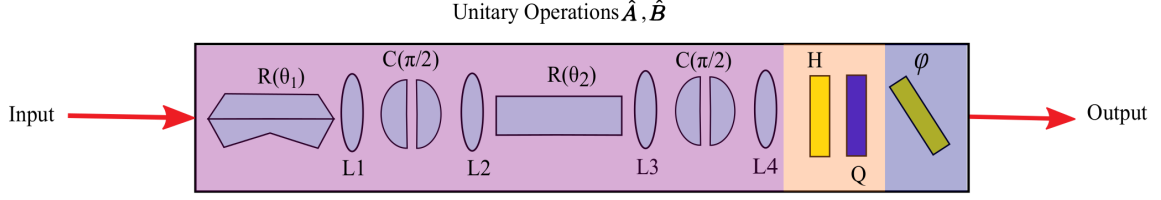


FIG. 3. Top view of the setup for realising the unitary operations  $\hat{A}$  and  $\hat{B}$  using a set of special inverting prisms  $R$ , and pairs of cylindrical lenses  $C$ . The prisms rotate the incoming transverse mode, effectively implementing the rotation  $R(\theta) = \begin{pmatrix} \cos 2\theta & \sin 2\theta \\ \sin 2\theta & -\cos 2\theta \end{pmatrix}$  in the  $\{|HG_{10}\rangle, |HG_{01}\rangle\}$  qubit subspace. The cylindrical lenses give a  $\pi/2$  relative phase shift to Hermite-Gaussian components of the incoming photon, effectively implementing  $C(\pi/2) = \begin{pmatrix} 1 & 0 \\ 0 & i \end{pmatrix}$ . The spherical lenses ( $L$ ) are used for mode-matching. The half-waveplates ( $H$ ) and quarter-waveplates ( $Q$ ) are used to correct polarisation changes caused by reflections in the prisms and  $\varphi$  represents a phase plate. The unitary operations of our interest are realised by varying the angles  $\theta_1$  and  $\theta_2$ . For example, in the figure  $R(\theta_1)$  is rotated by  $45^\circ$  and for  $R(\theta_2)$ , the angle is set at  $0^\circ$ . With a  $0^\circ$  global phase, the above setup represents an  $\hat{X}$  operation which transforms an input Hermite-Gaussian  $HG_{10}$  beam to a Hermite-Gaussian  $HG_{01}$  (see Supplemental Material).

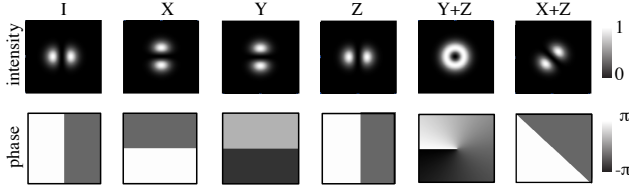


FIG. 4. Spatial transformations. The result of the unitaries acting on an input spatial mode of  $HG_{10}$  are also first-order spatial modes.

There are two main sources of errors in our experiment: rotational misalignments and imperfect mode matching. The inverting prisms are mounted on manual rotation

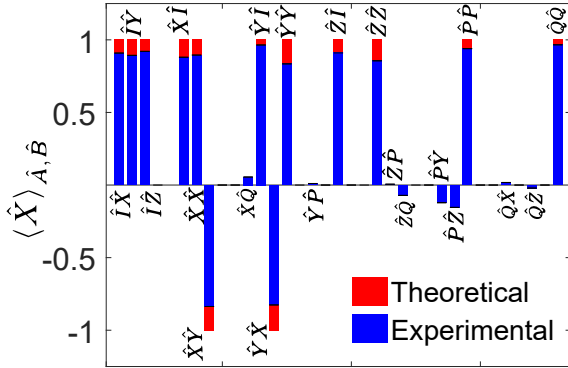


FIG. 5. Stokes parameters  $\langle \hat{X} \rangle_{\hat{A}, \hat{B}}$  obtained by measuring the polarisation of the output control qubit in the diagonal basis. The red bars show the ideal, theoretical values and the blue bars are the experimentally measured values. The unitary combinations are defined by combining the unitary operations at the top arm ( $\hat{A}$ ) and the bottom ( $\hat{B}$ ) arm, maintaining the order  $\hat{I}, \hat{X}, \hat{Y}, \hat{Z}, \hat{P} = \frac{\hat{Y} + \hat{Z}}{\sqrt{2}}$  and  $\hat{Q} = \frac{\hat{X} + \hat{Z}}{\sqrt{2}}$ . A Stokes parameter of  $+1$  means the output is diagonally polarised light,  $-1$  means it is anti-diagonally polarised light.  $1\sigma$  errors are too small to be visible in the plot.

stages with an uncertainty in angular position of  $1^\circ$ . Our witness is robust against these misalignments: accounting for these errors, one can derive a new corrected bound for causally separable processes, which we find to be close enough to zero that we still have room to obtain an experimental value below it (see Supplemental Material). The imperfect mode-matching degrades the visibility of the interference of the spatial modes, which is then reflected in the values of the Stokes parameters that we obtain. We have modelled these imperfections and predict an expectation value for our causal witness within the range  $-0.20 \lesssim \langle S \rangle \lesssim -0.14$ , higher than the theoretical value of  $\langle S \rangle \simeq -0.248$  calculated for an ideal switch.

We experimentally obtain a value of  $\langle S \rangle = -0.171 \pm 0.009$ , within our expected range, and 18 standard deviations from the bound  $\langle S \rangle \geq 0$  satisfied by all causally separable processes. Taking into account misalignment errors, the measured value is still 14 standard deviations below the corrected bound of  $\langle S \rangle \geq -0.038$  for causally separable processes obtained in the Supplemental Material. This confirms that the measured process is causally nonseparable, i.e., that it has no definite causal order, with an implementation free of the spatial and temporal loopholes that were left open in previous experiments [11, 12, 27].

Our architecture offers promising routes for further experimental investigations. Having polarisation as the control degree of freedom enables using polarisation-entanglement—which can be of very high quality, e.g. reaching a tangle of  $T = 0.987$  [28]—as the control for entangling the causal order of different quantum switches [10, 27]. Having transverse spatial modes as the target degree of freedom enables encoding qudits—as opposed to qubits—for investigating quantum communication with indefinite causal order in larger Hilbert space dimensions [5, 8]. Challenges for future demonstrations include realising quantum switches that put more than two events in an indefinite causal order, and physically

separating the control and target systems.

*Acknowledgements.* We thank Alastair A. Abbott for useful feedback on our manuscript. This work has been supported by: the Australian Research Council (ARC) by DECRA grants for FC (DE170100712) and JR (DE160100409), and the Centre of Excellence for Engineered Quantum Systems (EQUS, CE170100009); the French National Research Agency by the “Retour Post-Doctorants” program (ANR-13-PDOC-0026) for CB; the University of Queensland by a Vice-Chancellors Senior Research and Teaching Fellowship for AGW; and the John Templeton Foundation (the opinions expressed in this publication are those of the authors and do not necessarily reflect the views of the John Templeton Foundation). We acknowledge the traditional owners of the land on which the University of Queensland is situated, the Turrbal and Jagera people.

---

\* cyril.branciard@neel.cnrs.fr

† jacq.romero@gmail.com

‡ agx.white@gmail.com

- [1] G. Chiribella, G. M. D’Ariano, P. Perinotti, and B. Valiron, *Phys. Rev. A* **88**, 022318 (2013), arXiv:0912.0195 [quant-ph].
- [2] O. Oreshkov, F. Costa, and Č. Brukner, *Nat. Commun.* **3**, 1092 (2012), arXiv:1105.4464 [quant-ph].
- [3] M. Araújo, F. Costa, and Č. Brukner, *Phys. Rev. Lett.* **113**, 250402 (2014), arXiv:1401.8127 [quant-ph].
- [4] A. Feix, M. Araújo, and Č. Brukner, *Phys. Rev. A* **92**, 052326 (2015), arXiv:1508.07840 [quant-ph].
- [5] P. A. Guérin, A. Feix, M. Araújo, and Č. Brukner, *Phys. Rev. Lett.* **117**, 100502 (2016), arXiv:1605.07372 [quant-ph].
- [6] G. Chiribella, *Phys. Rev. A* **86**, 040301 (2012), arXiv:1109.5154 [quant-ph].
- [7] T. Colnaghi, G. M. D’Ariano, S. Facchini, and P. Perinotti, *Phys. Lett. A* **376**, 2940 (2012), arXiv:1109.5987 [quant-ph].
- [8] D. Ebler, S. Salek, and G. Chiribella, (2017), arXiv:1711.10165 [quant-ph].
- [9] L. Hardy, *J. Phys. A: Math. Gen.* **40**, 3081 (2007), arXiv:gr-qc/0608043.
- [10] M. Zych, F. Costa, I. Pikovski, and Č. Brukner, (2017), arXiv:1708.00248 [quant-ph].
- [11] L. M. Procopio, A. Moqanaki, M. Araújo, F. Costa, I. A. Calafell, E. G. Dowd, D. R. Hamel, L. A. Rozema, Č. Brukner, and P. Walther, *Nat. Commun.* **6**, 7913 (2015), arXiv:1412.4006 [quant-ph].
- [12] G. Rubino, L. A. Rozema, A. Feix, M. Araújo, J. M. Zeuner, L. M. Procopio, Č. Brukner, and P. Walther, *Sci. Adv.* **3**, e1602589 (2017), arXiv:1608.01683 [quant-ph].
- [13] M. Araújo, C. Branciard, F. Costa, A. Feix, C. Giarmatzi, and Č. Brukner, *New J. Phys.* **17**, 102001 (2015), arXiv:1506.03776 [quant-ph].
- [14] C. Branciard, *Sci. Rep.* **6**, 26018 (2016), arXiv:1603.00043 [quant-ph].
- [15] O. Oreshkov and C. Giarmatzi, *New J. Phys.* **18**, 093020 (2016), arXiv:1506.05449 [quant-ph].
- [16] F. Costa and S. Shrapnel, *New J. Phys.* **18**, 063032 (2016), arXiv:1512.07106 [quant-ph].
- [17] M.-D. Choi, *Linear Algebra Appl.* **12**, 95 (1975).
- [18] A. Jamiolkowski, *Rep. Math. Phys.* **3**, 275 (1972).
- [19] G. Gutoski and J. Watrous, in *Proceedings of 39th ACM STOC* (2006) pp. 565–574, arXiv:quant-ph/0611234.
- [20] G. Chiribella, G. M. D’Ariano, and P. Perinotti, *Phys. Rev. A* **80**, 022339 (2009), arXiv:0904.4483 [quant-ph].
- [21] S. Shrapnel, F. Costa, and G. Milburn, (2017), arXiv:1702.01845 [quant-ph].
- [22] J. Romero, D. Giovannini, M. G. McLaren, E. J. Galvez, A. Forbes, and M. J. Padgett, *J. Opt.* **14**, 085401 (2012).
- [23] J. Leach, J. Courtial, K. Skeldon, S. M. Barnett, S. Franke-Arnold, and M. J. Padgett, *Phys. Rev. Lett.* **92**, 013601 (2004).
- [24] C. Tamm and C. Weiss, *J. Opt. Soc. Amer. B* **7**, 1034 (1990).
- [25] M. W. Beijersbergen, L. Allen, H. V. der Veen, and J. P. Woerdman, *Opt. Commun.* **96**, 123 (1993).
- [26] D. L. Sullivan, *Appl. Opt.* **11**, 2028 (1972).
- [27] G. Rubino, L. A. Rozema, F. Massa, M. Araújo, M. Zych, Č. Brukner, and P. Walther, (2017), arXiv:1712.06884 [quant-ph].
- [28] A. Fedrizzi, T. Herbst, A. Poppe, T. Jennewein, and A. Zeilinger, *Opt. Express* **15**, 15377 (2007), arXiv:0706.2877 [quant-ph].
- [29] M. J. Padgett and J. P. Lesso, *J. Mod. Opt.* **46**, 175 (1999).

## SUPPLEMENTAL MATERIAL

### Construction of our causal witness

In this section we provide theoretical details for the construction of the causal witness we measure in our experiment. We recall that a causal witness is a Hermitian operator  $S$  for which  $\text{Tr}[SW] \geq 0$  for all  $W \in \mathcal{W}_{\text{sep}}$ , where  $\mathcal{W}_{\text{sep}}$  is the closed convex cone of (nonnormalised) causally separable process matrices. The search for a causal witness for a given causally nonseparable process matrix such as  $W_{\text{switch}}$  can be cast as a SemiDefinite Programming (SDP) problem that can be solved efficiently using convex optimisation techniques [13, 14].

In order to construct a causal witness for the quantum switch, we first need to specify its process matrix  $W_{\text{switch}}$ . As detailed in Refs. [13, 15], it can be written as

$$W_{\text{switch}} = \text{Tr}_{T_I} |w\rangle\langle w|$$

$$\text{with } |w\rangle = \frac{1}{\sqrt{2}} \left( |\psi\rangle_t^{A_I} \otimes |\mathbb{1}\rangle^{A_O B_I} \otimes |\mathbb{1}\rangle^{B_O T_I} \otimes |0\rangle_c^{C_I} + |\psi\rangle_t^{B_I} \otimes |\mathbb{1}\rangle^{B_O A_I} \otimes |\mathbb{1}\rangle^{A_O T_I} \otimes |1\rangle_c^{C_I} \right), \quad (\text{S1})$$

where  $|\psi\rangle_t$  is the initial state of the target qubit,  $|\mathbb{1}\rangle^{A_O B_I} = |0\rangle^{A_O} \otimes |0\rangle^{B_I} + |1\rangle^{A_O} \otimes |1\rangle^{B_I}$  represents an identity channel from  $A$ ’s outgoing space to  $B$ ’s incoming space for the target qubit, and similarly for

$|\mathbb{1}\rangle^{B_O T_I}, |\mathbb{1}\rangle^{A_O B_I}$  and  $|\mathbb{1}\rangle^{A_O T_I}$ , while  $|0\rangle_c$  and  $|1\rangle_c$  are the two orthogonal states of the control qubit that define the order between  $A$  and  $B$ ; see Fig. 1. In Eq. (S1) the superscripts ( $A_I, A_O$ , etc.) specify the Hilbert spaces in which each term is defined. In particular,  $C_I$  refers to the Hilbert space of the control qubit, which is measured at the output of the quantum switch, in  $C$ ;  $T_I$  refers to the Hilbert space of the target qubit at the output of the switch, which is not measured and thus traced out in  $W_{\text{switch}}$  (where  $\text{Tr}_{T_I}$  denotes the corresponding partial trace). The process matrix  $W_{\text{switch}}$  thus defined lives in the space  $A_I \otimes A_O \otimes B_I \otimes B_O \otimes C_I$ ; it can be verified that its trace is 4, equal to the product of the dimensions of  $A$  and  $B$ 's outgoing spaces (note that in the quantum switch,  $C$  has no outgoing space—or equivalently, a trivial 1-dimensional one) [2, 13, 15].

The set  $\mathcal{S}$  of causal witnesses  $S$ , such that  $\text{Tr}[SW] \geq 0$  for all causally separable process matrices  $W$ , is simply the dual of the cone  $\mathcal{W}_{\text{sep}}$  (with respect to the Hilbert-Schmidt inner product defined by the trace). It is also a closed convex cone, and was characterized in Refs. [13, 14] in terms of linear and semidefinite constraints for the case of interest for the quantum switch, where  $\mathcal{W}_{\text{sep}}, \mathcal{S} \subset A_I \otimes A_O \otimes B_I \otimes B_O \otimes C_I$ . In order to prove the causal nonseparability of the quantum switch, it suffices to find a witness  $S \in \mathcal{S}$  such that  $\text{Tr}[SW_{\text{switch}}] < 0$ . One may however want to optimise the choice of the witness in terms of its resistance to experimental noise. As shown in Refs. [13, 14], this can be done by minimising  $\text{Tr}[SW_{\text{switch}}]$  over the cone  $\mathcal{S}$ . Fixing the value  $\text{Tr}[S]$  to 8 (the product of the dimensions of  $A, B$  and  $C$ 's incoming spaces) ensures that the optimisation does not diverge to  $-\infty$ , and provides a practical interpretation for the optimal value of  $-\text{Tr}[SW_{\text{switch}}]$  obtained as a result of the optimisation, as the random robustness of  $W_{\text{switch}}$  with respect to white noise—i.e.,  $-\text{Tr}[SW_{\text{switch}}]$  is the minimal value of  $r$  that makes  $\frac{1}{1+r}(W_{\text{switch}} + r\hat{I}/8)$  causally separable, where  $\hat{I}/8$  represents here a maximally mixed state received by  $A, B$  and  $C$ .

The optimisation just described is a SDP problem. Further constraints can also be imposed on  $S$ . In our experiment, we want to be able to measure  $S$  by letting  $A$  and  $B$  only implement unitaries  $\hat{A}, \hat{B}$  taken from the set  $\mathcal{U} = \{\hat{I}, \hat{X}, \hat{Y}, \hat{Z}, \hat{P} = \frac{\hat{Y} + \hat{Z}}{\sqrt{2}}, \hat{Q} = \frac{\hat{X} + \hat{Z}}{\sqrt{2}}\}$ , and by letting  $C$  perform a measurement of  $\hat{X}$  (see main text). The statistics thus obtained allow us to calculate terms of the form  $\text{Tr}[(\mathcal{A} \otimes \mathcal{B} \otimes \hat{X}) W_{\text{switch}}]$ , for  $\hat{A}, \hat{B} \in \mathcal{U}$  (with  $\mathcal{A}, \mathcal{B}$  denoting their Choi representation). Note also that a trivial “measurement” of  $\hat{I}$  on the control qubit gives  $\text{Tr}[(\mathcal{A}' \otimes \mathcal{B}' \otimes \hat{I}) W_{\text{switch}}] = 1$  for any CP trace-preserving maps  $\mathcal{A}', \mathcal{B}'$ , so that such terms can also be trivially included in  $\text{Tr}[SW_{\text{switch}}]$ ; in fact it suffices to consider the term with  $\mathcal{A}' = \mathcal{B}' = \hat{I}/2$ . Our setup thus allows us to calculate  $\text{Tr}[SW_{\text{switch}}]$  for any witness of the form  $S = \frac{1}{4}(\hat{I} + \sum_{\hat{A}, \hat{B} \in \mathcal{U}} \gamma_{\hat{A}, \hat{B}} \mathcal{A} \otimes \mathcal{B} \otimes \hat{X})$  with

any real coefficients  $\gamma_{\hat{A}, \hat{B}}$ , which leads us to impose such a form in our optimisation problem.<sup>1</sup> Notice that we already included the constraint  $\text{Tr}[S] = 8$  by introducing the factor  $\frac{1}{4}$ , as  $\text{Tr}[\hat{I}] = 32$  for the identity operator  $\hat{I}$  acting here on the  $2^5$ -dimensional Hilbert space  $\mathcal{H}^{A_I} \otimes \mathcal{H}^{A_O} \otimes \mathcal{H}^{B_I} \otimes \mathcal{H}^{B_O} \otimes \mathcal{H}^{C_I}$ .

The causal witness we measure in the experiment is the result of the following SDP problem:

$$\begin{aligned} & \text{minimize } \text{Tr}[SW_{\text{switch}}] \\ & \text{such that } S = \frac{1}{4}(\hat{I} + \sum_{\hat{A}, \hat{B} \in \mathcal{U}} \gamma_{\hat{A}, \hat{B}} \mathcal{A} \otimes \mathcal{B} \otimes \hat{X}) \in \mathcal{S}, \\ & \gamma_{\hat{A}, \hat{B}} \in \mathbb{R}. \end{aligned} \quad (\text{S2})$$

The nonzero coefficients  $\gamma_{\hat{A}, \hat{B}}$  we thus obtained are listed in Table S1, together with the corresponding theoretically expected and experimentally measured values of the Stokes parameters  $\langle \hat{X} \rangle_{\hat{A}, \hat{B}}$ , that allow one to calculate the value of the causal witness,  $\langle S \rangle = 1 + \frac{1}{4} \sum_{\hat{A}, \hat{B}} \gamma_{\hat{A}, \hat{B}} \langle \hat{X} \rangle_{\hat{A}, \hat{B}}$  as in Eq. (5). The theoretically expected value is found to be  $\langle S \rangle = \text{Tr}[SW_{\text{switch}}] \simeq -0.248$ ; we experimentally obtained a value of  $\langle S \rangle = -0.171 \pm 0.009$  (which, as recalled, thus gives a value  $r = -\langle S \rangle = -0.171 \pm 0.009$  for the random robustness of our quantum switch [13, 14]).

### Implementation of unitaries

The six unitaries necessary for the calculation of our causal witness are:  $\hat{I} = \begin{pmatrix} 1 & 0 \\ 0 & 1 \end{pmatrix}$ ,  $\hat{X} = \begin{pmatrix} 0 & 1 \\ 1 & 0 \end{pmatrix}$ ,  $\hat{Y} = \begin{pmatrix} 0 & -i \\ i & 0 \end{pmatrix}$ ,  $\hat{Z} = \begin{pmatrix} 1 & 0 \\ 0 & -1 \end{pmatrix}$ ,  $\hat{P} = \frac{\hat{Y} + \hat{Z}}{\sqrt{2}} = \frac{1}{\sqrt{2}} \begin{pmatrix} 1 & -i \\ i & -1 \end{pmatrix}$  and  $\hat{Q} = \frac{\hat{X} + \hat{Z}}{\sqrt{2}} = \frac{1}{\sqrt{2}} \begin{pmatrix} 1 & 1 \\ 1 & -1 \end{pmatrix}$ .

To implement these unitaries we used the setup shown in Fig. 3.  $C(\pi/2)$  is a mode-converter which shifts the Hermite-Gaussian mode  $\text{HG}_{01}$  by  $\pi/2$  out of phase with respect to the Hermite-Gaussian  $\text{HG}_{10}$  component.  $R(\theta)$  is a M-shaped rotating prism oriented at a physical angle  $\theta$ , which reflects and rotates an incoming beam by  $2\theta$ . These are represented by the following matrices:  $C(\pi/2) = \begin{pmatrix} 1 & 0 \\ 0 & i \end{pmatrix}$  and  $R(\theta) = \begin{pmatrix} \cos 2\theta & \sin 2\theta \\ \sin 2\theta & -\cos 2\theta \end{pmatrix}$ . We started with an  $\text{HG}_{10}$  mode prepared as in Fig. S1, using a cover slip to impart a  $\pi$ -phase shift to half of an incoming  $\text{HG}_{00}$  beam, and encoded our target qubit in

<sup>1</sup> We also checked that with our choice of unitary operations for  $A$  and  $B$ , allowing for measurements of  $\hat{Y}$  or  $\hat{Z}$  on the control qubit in  $C$ —i.e., also adding terms of the form  $\gamma_{\hat{A}, \hat{B}}^Y \mathcal{A} \otimes \mathcal{B} \otimes \hat{Y}$  and  $\gamma_{\hat{A}, \hat{B}}^Z \mathcal{A} \otimes \mathcal{B} \otimes \hat{Z}$  in  $S$ —does not help further decrease the value of  $\text{Tr}[SW_{\text{switch}}]$  in our optimisation problem (S2).



$\hat{A}$	$\hat{B}$	$\gamma_{\hat{A},\hat{B}}$	$\langle \hat{X} \rangle_{\hat{A},\hat{B}}^{\text{theor.}}$	$\langle \hat{X} \rangle_{\hat{A},\hat{B}}^{\text{exp.}}$
$\hat{I}$	$\hat{X}$	-0.1967	1	$0.9090 \pm 0.0003$
	$\hat{Y}$	-0.1967	1	$0.8931 \pm 0.0003$
	$\hat{Z}$	-0.2775	1	$0.9208 \pm 0.0003$
$\hat{X}$	$\hat{I}$	-0.1967	1	$0.8801 \pm 0.0004$
	$\hat{X}$	-0.2572	1	$0.8952 \pm 0.0003$
	$\hat{Y}$	0.2332	-1	$-0.8365 \pm 0.0004$
$\hat{Y}$	$\hat{Q}$	0.5143	0	$0.0553 \pm 0.0007$
	$\hat{I}$	-0.1967	1	$0.9647 \pm 0.0002$
	$\hat{X}$	0.2332	-1	$-0.8259 \pm 0.0004$
$\hat{Z}$	$\hat{Y}$	-0.2572	1	$0.8346 \pm 0.0004$
	$\hat{P}$	0.5143	0	$0.0107 \pm 0.0008$
	$\hat{I}$	-0.2775	1	$0.9099 \pm 0.0003$
$\hat{P}$	$\hat{Z}$	-0.6131	1	$0.8558 \pm 0.0004$
	$\hat{P}$	0.5143	0	$0.0059 \pm 0.0008$
	$\hat{Q}$	0.5143	0	$-0.0714 \pm 0.0007$
$\hat{Q}$	$\hat{Y}$	0.5143	0	$-0.1217 \pm 0.0007$
	$\hat{Z}$	0.5143	0	$-0.1539 \pm 0.0007$
	$\hat{P}$	-1.0286	1	$0.9394 \pm 0.0002$
$\hat{Q}$	$\hat{X}$	0.5143	0	$0.0177 \pm 0.0007$
	$\hat{Z}$	0.5143	0	$-0.0209 \pm 0.0008$
	$\hat{Q}$	-1.0286	1	$0.9659 \pm 0.0002$

TABLE S1. Data for the different combinations of unitary operations  $\hat{A}$  and  $\hat{B}$ . The coefficients  $\gamma_{\hat{A},\hat{B}}$  were obtained by solving the semidefinite programming problem described in Eq. (S2) (for the combinations of  $\hat{A}$  and  $\hat{B}$  not shown in the table, the SDP returned a null coefficient  $\gamma_{\hat{A},\hat{B}} = 0$ , up to numerical precision). The expectation value  $\langle \hat{X} \rangle_{\hat{A},\hat{B}}$  of the polarisation measurement on the control qubit after the unitaries  $\hat{A}$  and  $\hat{B}$  were applied is effectively a Stokes parameter. Together with  $\gamma_{\hat{A},\hat{B}}$ , the table lists both the theoretically expected values,  $\langle \hat{X} \rangle_{\hat{A},\hat{B}}^{\text{theor.}}$ , and the experimentally measured values,  $\langle \hat{X} \rangle_{\hat{A},\hat{B}}^{\text{exp.}}$ , of this Stokes parameter. Error bars ( $1\sigma$ ) were calculated by propagation of error on the individual Stokes parameter with Poissonian counting statistics.

the spatial mode such that  $|\text{HG}_{10}\rangle = |0\rangle = \begin{pmatrix} 1 \\ 0 \end{pmatrix}$  and  $|\text{HG}_{01}\rangle = |1\rangle = \begin{pmatrix} 0 \\ 1 \end{pmatrix}$ . After spatial Fourier filtering, a HWP was used to set the polarisation of the control.

The transformation performed by each box  $A$  and  $B$  (for a beam propagating from left to right in Fig. 3) can be written as

$$U(\varphi, \theta_1, \theta_2) = e^{i\varphi} C(\pi/2) R(\theta_2) C(\pi/2) R(\theta_1), \quad (\text{S3})$$

where the global phase  $\varphi$  can be imparted by a tilted phase plate which is placed only when  $\hat{I}$  is one of the operations. The rotating prisms act like a quarter-waveplate, shifting one linear polarisation by  $\pi/2$  out of phase with respect to the other, hence a combination of a HWP and a QWP are used for polarisation correction. The cylindrical lens pairs in this implementation are fixed, and placed in between two spherical lenses to match the beam waists to that required by the mode-converters [29]. We only

have two rotating components, the two inverting prisms. This is enough to implement the six unitaries as listed above given the following angles and phases as shown in Table S2.

Unitary	$\varphi$	$\theta_1$	$\theta_2$
$\hat{I}$	$-\frac{\pi}{2}$	$\frac{\pi}{4}$	$\frac{\pi}{4}$
$\hat{X}$	0	$\frac{\pi}{4}$	0
$\hat{Y}$	0	0	$\frac{\pi}{4}$
$\hat{Z}$	0	0	0
$\hat{P}$	0	0	$\frac{\pi}{8}$
$\hat{Q}$	0	$\frac{\pi}{8}$	0

TABLE S2. Phases and angles for the unitary operations realised in our experiment, given by Eq. (S3).

### Taking experimental imperfections into account

Because of experimental imperfections in the operations that take place at events  $A$ ,  $B$  and  $C$ , the witness measured in the experiment does not exactly match the ideal one. Therefore, it is in principle possible that the expectation value  $\langle S_{\text{exp}} \rangle$  of the experimentally measured witness  $S_{\text{exp}}$ , calculated from the observed statistics through Eq. (5), is negative for some causally separable process. This means that strictly speaking, an experimental negative value cannot be taken as a proof of causal nonseparability. To go around this problem, we derived a corrected causal bound  $b < 0$  such that  $\text{Tr}[S_{\text{exp}} W_{\text{sep}}] \geq b$  for all causally separable process matrices  $W_{\text{sep}}$ , where  $S_{\text{exp}}$  is estimated based on our understanding of the source of the experimental imperfections.

The main source of errors in the implementation of the unitaries lies in setting the angles of each optical element that realises the unitaries. We estimate the new causal bound with a simulation of our experimental causal wit-

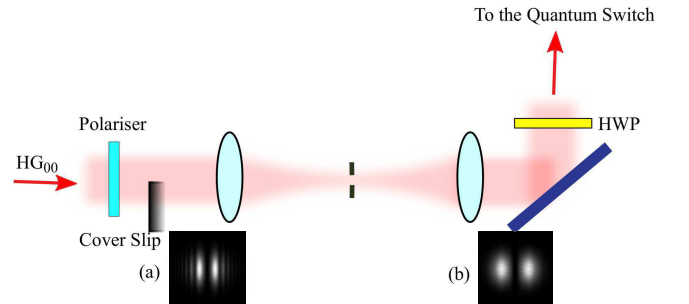


FIG. S1. Preparation method for our input state. We started with a horizontally polarised fundamental Gaussian mode (HG<sub>00</sub>). We placed a cover slip to introduce a  $\pi$ -phase shift to half of the beam. The resulting beam is a superposition of odd-order Hermite-Gaussian modes, as shown in (a). The higher order modes are eliminated by performing a spatial filtering on the beam, the resulting beam is in the HG<sub>10</sub> mode, as shown in (b). The HWP is used to make the beam diagonally polarised.

ness  $S_{\text{exp}}$ , adding errors of  $1^\circ$  to the angles of each optical element in the unitaries and looking for the combination that minimises  $b$  (i.e., the worst-case scenario within the expected range of errors). We find that our witness is sufficiently robust to these errors: we varied randomly (up to  $\pm 1^\circ$ ) the angles of each optical element in the unitaries and estimated the new causal bound with the

following SDP:

$$\begin{aligned} & \text{minimize } \text{Tr}[S_{\text{exp}}W] \\ & \text{such that } W \in \mathcal{W}_{\text{sep}}. \end{aligned} \tag{S4}$$

Using our simulation of the experimental witness  $S_{\text{exp}}$ , we ran 1000 different configurations of the experimental angles having errors of up to  $\pm 1^\circ$ . When we set the errors in the angles with a random sign, and a random, uniformly distributed, amplitude in  $[0, 1]$ , we reached a minimum value of  $b = -0.029$ ; when the errors had a random sign but a fixed amplitude of  $1^\circ$  the minimum value was  $b = -0.038$ . Our measured value is still below these bounds.